Dislocation structure of a defective near-surface skin layer in V_2H

J. Trenkler,[1,3] R. Barabash,[2,3] H. Dosch,[3] and S. C. Moss[1]
[1]*Department of Physics, University of Houston, Houston, Texas 77204-5506*
[2]*Metals & Ceramics Div., ORNL, Oak Ridge, Tennessee 37831-6118*
[3]*Max-Planck-Institut für Metallforschung, D-70569 Stuttgart, Germany*
(Received 18 April 2001; published 1 November 2001)

Here we present a detailed analysis of the depth-dependent dislocation substructure responsible for the graded defective ''skin layer'' in single crystal V_2H whose phase transition appears continuous (tricritical) in this skin layer and strongly first order in the bulk. A skin layer with an effective thickness of 5–10 μm is located just below the surface of a ~1-mm-thick bulk crystal. Within this skin, the conventional mosaic spread (x-ray rocking curve) shows a full width at half maximum that decays into the bulk. In this paper, we determine, via diffuse scattering distribution in the vicinity of the Bragg points, the dislocation arrangement and its associated stress field. The results can then be used in interpreting the influence of this stress field on the change of the order of the phase transition as well as in the discussion of the two-length scale pattern where both length scales show a critical behavior.

DOI: 10.1103/PhysRevB.64.214101 PACS number(s): 61.10.−i, 61.72.Bb, 61.72.Dd, 61.72.Lk

In a series of papers, we have explored the unusual scattering associated with the phase transition in V_2H from a disordered bct β_2-phase above the transition temperature of $T_C \approx 445$ K to an ordered monoclinic β_1 phase below T_C. The ordering takes place on the octahedral sites of the vanadium (V) lattice. When preparing the crystal, the ordering tends to select one of the three cubic axes due to the particular choice of the sample geometry (a thin ~1-mm-thick single-crystal V plate) and the hydrogen (H-) loading conditions, thereby creating a pseudotetragonal z axis.[1–3] This leads to the exclusive occupation of one subset of octahedral sites in the β_1 and β_2 phases which are usually referred to as O_Z sites. At the concentration of V_2H, one-half of the O_Z sites are filled. In the disordered bct phase, the two sublattices of the O_Z sites, namely O_{Z1} and O_{Z2} sites, are equally occupied. Below the ordering transition, the O_{Z1} sites become increasingly occupied with decreasing temperature. The exclusive occupation of O_{Z1} sites in every other $(0\,1\,\bar{1})$ plane leads to a periodic distortion of the vanadium host lattice and thus to $\{0\,h/2\,\bar{h}/2\}$ superstructure peaks (pseudo-bct notation) (See Refs. 1 and 4–6 for both a detailed description of the structure and earlier results.) The structure factor of the superstructure reflections can be expressed in terms of the modulated distortion of the V-lattice planes, and their relative occupancy is directly related to the Bragg-Williams long-range order parameter Φ.[4,5]

The critical behavior of this transition was extensively studied with x-rays both in Ref. 6 and Refs. 5, 7, and 8. The crystal of Ref. 6 was a large multidomain sample, and only the long-range order could be investigated. Nonetheless, the decay of the long-range order, $\Phi \propto (1 - T/T_C)^{\beta}$, in the crystals of both Ref. 6 and Refs. 5 and 8 was clearly continuous and considered to be of the tricritical class even though the critical exponent β was found to lie between 0.15 and 0.18, which was also found for other tricritical systems.[9–11]

In an earlier study,[7] the depth dependence of the critical behavior above T_C was further explored and, near T_C—a temperature determined by extrapolation of the full width at half maximum (FWHM) in the disordered state to the ordered peak width—both the susceptibility exponent γ and the correlation length exponent υ assumed their mean field values $\gamma = 0.96 \pm 0.16$ and $\upsilon = 0.52 \pm 0.06$, respectively, as expected for a tricritical point when approaching the phase-transition line perpendicularly. At larger reduced temperatures, $t = (T/T_C - 1)$, the exponents crossed over to larger values which were both unusual and clearly nonuniversal.

The most dramatic behavior, however, concerns our data on a bulk sample as first reported in Ref. 8. While the phase transition in a near surface volume of some μm thickness was continuous,[6,8] the transition in the bulk was clearly first order.[8] This was not due to a change in either the H or O concentration at the surface below a depth of ~200 Å (for a detailed discussion of this issue, see Ref. 5). Yet the thickness of the surface ''skin layer,'' within which a continuous tricritical behavior was seen, was of the order of 6–10 μm. Figure 1 shows the decay of the mosaic spread, i.e., the FWHM of the crystal rocking curves at a Bragg peak, versus the depth in from the surface. Since the small H and O gradients in the first 200 Å do not play any role here (see Refs. 5 and 12) the only remaining ''defects'' that we might then invoke to explain the unusual conversion of a bulk first-order transition to a continuous tricritical transition in this defective ''skin layer'' are the dislocation arrays that are responsible for the decay of mosaic spread as shown in Fig. 1. (This point was not made in Ref. 7, as our narrow radial scan led us tentatively to rule out dislocations and their associated strains.) In a purely formal sense, such a conversion may be understood using a Landau free energy F in which the free energy is written as an expansion out to the sixth order,

$$F = a\Phi^2 + b\Phi^3 + c\Phi^4 + d\Phi^6 - \Phi H/k_B T,$$

where a, b, c, and d may be analytical functions in T and H, $d > 0$ for simplicity, Φ the conjugate variable to the order parameter, H the applied field, k_B the Boltzmann constant, and T the temperature. In our alloy, a third-order term is not permitted by symmetry and, we must thus invoke a negative

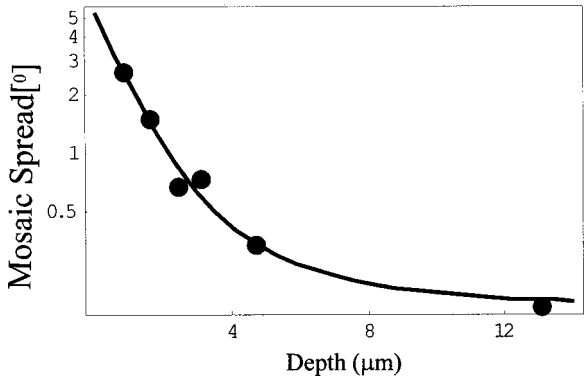

FIG. 1. Mosaic spread (logarithmic scale) vs effective penetration depth extracted from five different experiments with $E=5.9$, 9.0, 10.5, 11.95, and 17.5 keV(Mo $K\alpha 1$). The error bars are within the symbol size. The fit (solid line) is to the function $0.2+4.5e^{-x}+0.64e^{-x/3}$, where x is the vertical depth from the surface.

fourth-order term and a positive sixth-order term to obtain a first-order transition (if H is zero) (for an explicit treatment, see Ref. 12). To revert to a tricritical point, one thus need only change the sign of the fourth-order term to convert the phase transition from a tricritical transition to a discontinuous transition. There is a good deal of literature on this point, which invokes the influence of random bonds and random fields (see Ref. 13 and references therein). However, an applied (elastic) field may also accomplish the same result.[14] In this paper, we describe in some detail the depth dependent dislocation structure in our ''skin layer'' to which we must ultimately refer in explaining the change from discontinuous (first order) to tricritical behavior.

As noted earlier,[1,4,6] in V_2H, the hydrogen atoms occupy z axis octahedral interstitial positions in planes parallel to $(0\,1\,\bar{1})$, namely, the O_Z sites. The sample is in the form of a plate of thickness $\sim$1 mm. Both the edges and planes of this plate are normal to the $[0\,1\,\bar{1}]$ direction. Surface preparation consisted of a polish followed by an etching before loading with H at elevated temperatures. Of course, an oxide layer automatically reformed on cooling. This layer penetrates about 200–300 Å, and the H depletion extends to exactly the same depth and levels off at the independently measured bulk composition.[8] Thus the oxide formation, plus the residual polishing strain, is responsible for the defective skin layer and the attendant mosaic spread. Our data, i.e., probing the defective skin layer whose mosaic spread is shown in Fig. 1, is collected from the narrow (1 mm thick) $(0\,1\,\bar{1})$ crystal edge in reflection geometry. The bulk data taken in transmission geometry probe these same planes. Planes of the type $(0\,1\,\bar{1})$ are the glide planes for dislocations in a vanadium crystal with a typical Burgers vector $\frac{1}{2}[111]$. A random distribution of such dislocations would broaden the $(0\,1\,\bar{1})$ reflection in the radial direction. Such a broadening, however, was not observed experimentally. Nonetheless, the skin layer of V_2H is characterized by the enlarged mosaic spread decaying into the bulk, in an exponential manner, $0.2+4.5e^{-x}+0.64e^{-x/3}$, as shown in Fig. 1 (and Fig. 2 of Ref. 8). This phenomenological parameter (mosaic spread)

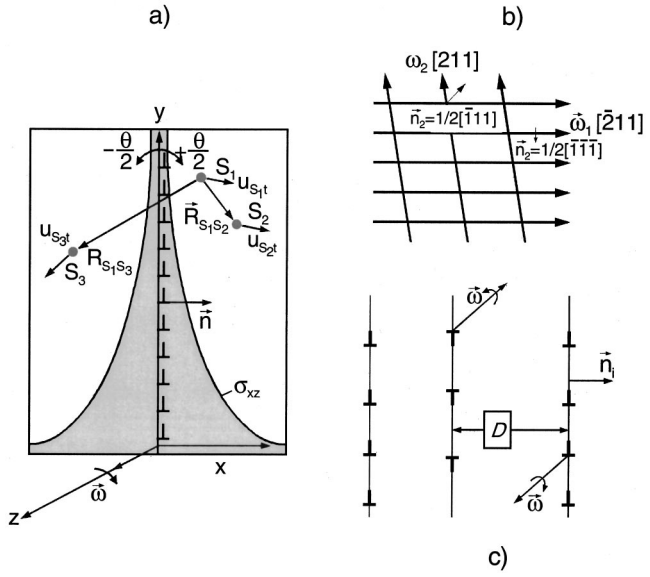

FIG. 2. Schematic representation of the dislocation walls in the defective skin layer at a constant depth. (a) Displacements, $\mathbf{u}_{st}$, of the scattering cells $\mathbf{s}_i$ in different positions with respect to the dislocation wall with two possible positions of the distance vector $\rho = R_{S_1S_2}$ (or $R_{S_1S_3}$) between them; the gray field shows the decay of the stress σ_{xy} with distance x from the dislocation wall. (b) Top view of the network of the dislocation walls and their orientation (for the notation, see the text). (c) Arrangement of dislocation walls with a mean separation D.

from a microscopic viewpoint can be attributed to a crystal with dislocation walls. A typical arrangement would be a structure with dislocation walls with an equidistant distribution of dislocations with Burgers vector $\frac{1}{2}[111]$ within the wall, thus providing pure rotation modes in the crystal as schematically shown in Fig. 2(a). The walls are arranged in such a way that they form a parallelogram-shaped set considered from a top view, i.e., in the $(0\,1\,\bar{1})$ plane. The orientation of these walls is shown in Fig. 2(b). The number of walls with Burgers vector $+\mathbf{b}$ and $-\mathbf{b}$ is assumed to be equal, as shown in Fig. 2(c). If the dislocation ensemble contains only such dislocation walls, it will result in the appearance of local rotation fields in the crystal. In this case, there will be practically no strain between them, which is associated with the translational component of the displacement field. The existence of dislocation walls changes the scattering distribution about fundamental Bragg reflections as well as long-range order superstructure reflections. Many of the considerations presented here will also directly affect the distribution of critical diffuse scattering at the superlattice positions above the transition temperature.

If the dislocations are regularly arranged inside the dislocation wall, they create a displacement field which is the same as that created by a single defect with a rotation field around the axis ω as shown in Figs. 2(a) and 2(c). The orientation of the wall is characterized by its normal, $\mathbf{n}=\langle\mathbf{111}\rangle$, and by the direction of rotation axis $\boldsymbol{\omega}=\langle\mathbf{211}\rangle$. The intensity distribution associated with this arrangement essentially depends on the ratio between the mean distance between dislocation walls, D, and the mean distance h between

dislocations *within* the wall in units of the interplanar spacing. To analyze the influence of a local rotation field on the scattering, we consider pure tilt boundaries formed by equidistant edge dislocations. The stress field σ_{xy} around such walls decreases exponentially with the distance from the wall[15] (see Fig. 2),

$$\sigma_{xy} \propto \frac{bx}{h^2} e^{-2\pi x/h} \cos\left(2\pi \frac{y}{h}\right),$$

where b is the magnitude of the vector **b**. It is this stress field and its gradient, which we believe to be essential to our understanding of the conversion of a first-order bulk transition to the tricritical transition in the defective skin layer. We again note that the data presented in this paper were taken exclusively in the defective skin layer.

If h_α is the distance between dislocations within the wall, one can consider this boundary as a single defect producing a local rotation field $\Theta_{sr\alpha}$ with a mean misorientation angle

$$\Theta_\alpha = b_\alpha / h_\alpha . \tag{1}$$

We now let $\mathbf{R}_{r\alpha} = R_r \mathbf{n}_\alpha$ be the vector between the wall r and a parallel plane containing the origin of the coordinate system (i.e., $\mathbf{n}_\alpha$ is a unit vector perpendicular to the plane of the wall containing the dislocation lines). The translation strains caused by the dislocation array decrease exponentially with the distance from the wall.[16] This results in different diffraction conditions for radial and for azimuthal directions.

If the planes of the dislocation walls in the skin layer are distributed randomly, the intensity distribution, following the approach in Refs. 17 and 18, may be described by

$$I(\mathbf{q}) \propto f^2 \sum_{s,s'} \exp(i\mathbf{q},\rho)\exp[-T(\mathbf{R}_s^0,\rho)],$$

$$T = \sum_\alpha c_\alpha \sum_\gamma [1-\exp(i\mathbf{Q}\cdot\mathbf{u}_{ss'r\alpha})], \tag{2}$$

where c_α is the concentration of α type dislocation walls, $\rho = \mathbf{R}_s^0 - \mathbf{R}_{s'}^0$ is the vector between two scattering cells s and s'. We emphasize that the influence of the dislocation walls on the scattering distribution is *only* characterized by the function T. The relative displacements $\mathbf{u}_{ss'}$ between them (due to the local rotation caused by the subboundaries [again see Fig. 2(a)] is then given by

$$\mathbf{u}_{ss'r_\alpha} = \mathbf{u}_{sr_\alpha} - \mathbf{u}_{s'r_\alpha} = \{c_{sr}[\omega_\alpha, \mathbf{R}_s^0 - \mathbf{R}_r] - c_{s'r}[\omega_\alpha, \mathbf{R}_{s'}^0 - \mathbf{R}_r]\}\Theta_\alpha . \tag{3}$$

There are two different possible mutual orientations of the scattering cells: in the first case, both cells are on one side of the wall (cells $s1$ and $s2$), while in the second case they are on different sides of the wall (cells $s1$ and $s3$) as shown in Fig. 2(a). The scalar product $\mathbf{Q}\cdot\mathbf{u}$ is then given by

$$\mathbf{Q}\cdot\mathbf{u}_{ss'r} = \pm\frac{b}{h}(\mathbf{Q}[\omega\times\boldsymbol{\rho}]), \tag{4a}$$

if, e.g., s_1 and s_2 cells are on one side of the wall, or

$$\mathbf{Q}\cdot\mathbf{u}_{ss'r} = -\frac{b}{h}(\mathbf{Q}[\omega\times(\mathbf{R}_s - \mathbf{R}_{s'} - 2\mathbf{R}_r)]), \tag{4b}$$

if, e.g., s_1 and s_3 cells are on opposite sides of the wall [Fig. 2(a)]. In the general case,

$$T(\mathbf{R}_s^0,\rho) = \mathrm{Re}\, T(\mathbf{R}_s^0,\rho) + i\ \mathrm{Im}\, T(\mathbf{R}_s^0,\rho). \tag{5}$$

For equal probabilities of the boundaries with opposite rotation angles, $\mathrm{Im}\, T(\rho) = 0$ and

$$T(\rho) = \sum_\alpha \frac{|\rho\mathbf{n}_\alpha|}{D_\alpha} + \sum_\alpha \frac{|\mathbf{R}_s^0\mathbf{n}_\alpha|}{D_\alpha}\{1-\cos[\mathbf{Q}(\omega_\alpha\times\rho\Theta_\alpha)]\}, \tag{6}$$

where D_α is the distance between the α-type walls. Such an expression for $T(\rho)$ results in a strong asymmetry of the intensity distribution $I(q)$ in the vicinity of the reciprocal lattice point $\mathbf{G}_{hkl}$, where hkl are conventional Miller indices in the tetragonal notation.

In the radial direction, this leads to a sharp Lorentzian shape of the intensity distribution

$$I(q_D) = I_{Di}\frac{q_{Di}}{\pi^2 q_D^2 + q_{Di}^2}, \tag{7}$$

where q_D is the deviation of the diffraction vector from the exact Bragg position in the radial direction. Here the integral linewidth, as commonly used, is given by $q_{Di} = \pi\varsigma/D$, (or in angular units by $2\delta\theta = \varsigma\lambda \sec\theta/D$), where D is the average distance between dislocations as in Fig. 2. The orientation factor in the radial direction can be written as

$$\varsigma = \Sigma_\alpha |(\mathbf{m}\cdot\mathbf{n}_\alpha)|. \tag{8}$$

The factor ς is determined by both the orientations of the wall and by the diffraction vector $\mathbf{Q}$; $\mathbf{m} = \mathbf{Q}/|\mathbf{Q}|$. Such a dependence for radial line broadening corresponds to classical ''particle-size broadening.''

The azimuthal intensity distribution $I(q_\xi)$, corresponding, for instance, to the rocking curve related to the main axis ξ of the azimuthal plane, is described by

$$I(q_\xi) = \frac{2\pi f^2}{v^2(Q\Theta)^2\zeta} \times \int d\mathbf{R}_s^0 \frac{D}{R_s^0\sqrt{A_{\xi\xi}A_{\eta\eta}}} \exp\left(-\frac{D}{4R_s^0(Q\Theta)^2}\frac{q_\xi^2}{A_{\xi\xi}}\right), \tag{9}$$

where v is the volume of the unit cell, and f the scattering amplitude. The matrix $A_{\eta\xi}$ depends on the mutual orientations between the diffraction vector $\mathbf{Q}$ and the directions τ_α of the dislocation lines inside the walls in the azimuthal plane (perpendicular to the diffraction vector). $A_{\eta\xi}$ may thus be viewed as an azimuthal orientation factor. The integral width in the azimuthal plane is then given by

$$\delta q_\perp = \sqrt{2\pi A_{\xi\xi}}\sqrt{\tfrac{L}{D}}\Theta Q. \tag{10}$$

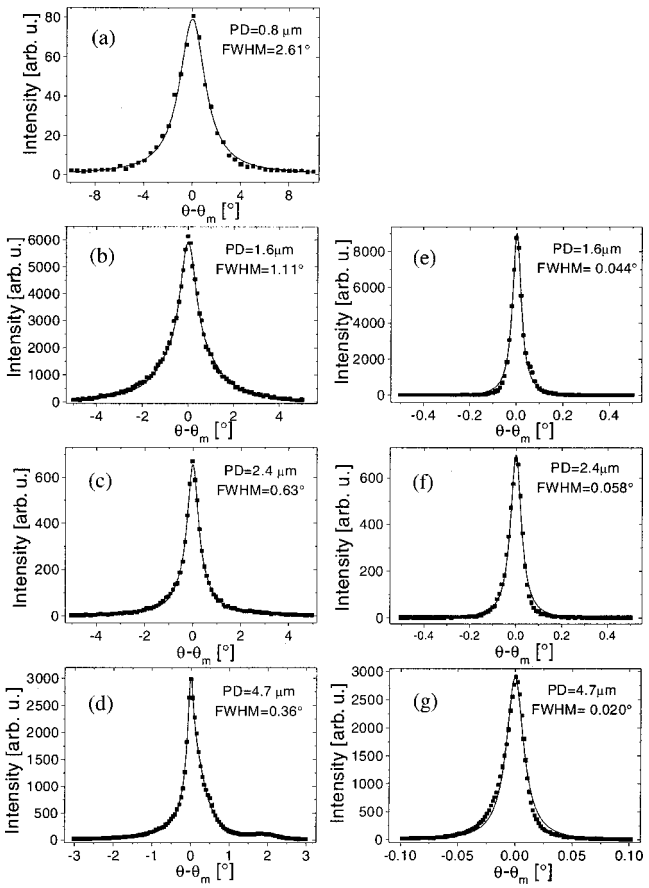

FIG. 3. Experimental rocking curves (a)–(d) and radial curves (e)–(g), taken at different x-ray energies and momentum transfers yielding different penetration depths. (a) corresponds to the $(0\ 1/2\ \overline{1/2})$ reflection taken at $E=5.9$ keV; (b) and (e) to $(0\ 1\ \overline{1})$ at $E=5.9$ keV; (c) and (f) to $(0\ 3/2\ \overline{3/2})$ at $E=5.9$ keV; and (d) and (g) to $(0\ 3/2\ \overline{3/2})$ at $E=9.0$ keV.

In the simple case of two different sets of dislocation walls with equal Burgers vector in the crystal, the scattering contours around the points $\mathbf{G}_{hkl}$ will have the shape of thin disks considerably more extended in the azimuthal plane than in the radial direction.

A set of experimental rocking curves around selected fundamental and superlattice reflections are shown in Fig. 3, in which the most shallow penetration depth in our skin layer showed the greatest azimuthal (rocking) breath. The results of our simulation, obtained for the scattered intensity of our crystal with two sets of dislocation walls, having the orientations of the rotation axes ω_1 and ω_2 of the wall corresponding to Fig. 2(b), are shown in Fig. 4. The decrease of the misorientation angle of each dislocation wall with depth reduces the broadening in the rocking, i.e., mosaic, direction without changing its shape. The input of each set of dislocation walls into the intensity distribution of each reflection essentially depends on the orientation factors. These are clearly different in radial and rocking directions of reciprocal space.

After the simulation of the intensity distribution for many different sets of possible dislocation wall orientations, and

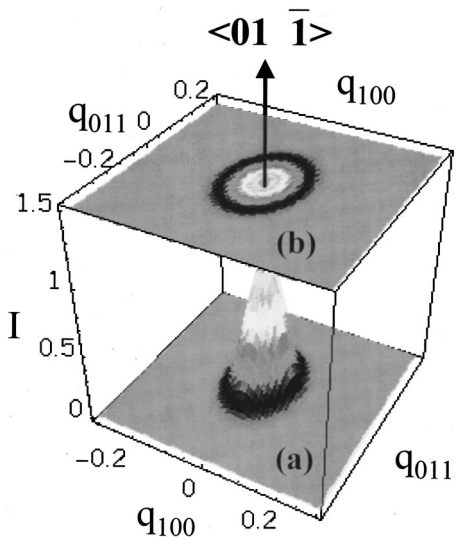

FIG. 4. Simulated 3D intensity portrait (a) and its projection in the transverse plane, forming a contour map (b), in the azimuthal plane around the $(01\ \overline{1})$ reflection at a penetration depth of about 2.4 μm. $\mathbf{q}_{011}$ corresponds to the [011] rocking direction and $\mathbf{q}_{100}$ to the [100] rocking direction. It is clear from Figs. 3 and 4 that the scattering is isotropic in the transverse plane, but resolution limited in the radial $(01\ \overline{1})$ direction. The images are shown on the frame of a cube simply for convenience.

comparing the radial and rocking peak widths with the experimental ones, we were able to conclude that in the defective skin layer, there remain essentially two sets of dislocation walls. These sets create a net of domain walls whose misorientation decays with increasing depth into the bulk. The following orientations for these two sets were found:

$$\mathbf{n}_1=\tfrac{1}{2}[\overline{1\ 1\ 1}],\quad \boldsymbol{\omega}_1=\tfrac{1}{6}[2\ 1\ 1], \tag{11a}$$

$$\mathbf{n}_2=\tfrac{1}{2}[\overline{1}\ 1\ 1],\quad \boldsymbol{\omega}_2=\tfrac{1}{6}[\overline{2}11]. \tag{11b}$$

For such a geometry of the dislocation walls, Eq. (8) yields an orientation factor $\zeta=0$ in radial direction for any $(0\ 1\ \overline{1})$-type reflection. This implies that the intensity distribution should correspond to the resolution function in the radial direction, which is observed in the experiments.

Within the rocking plane, such a net of dislocation walls gives a broad intensity distribution. The 3D portrait of this intensity distribution and the corresponding contour map for a misorientation angle $\Theta=0.0025$ rad at a depth of 2.4 μm are shown in Fig. 4.

From the experimental and simulated rocking curves, we were able to quantitatively determine the misorientation angle created by each dislocation wall as well as the distance h, where h/a is the number of interatomic distances, a, between neighboring dislocations in the wall for different depths, as shown in Fig. 5; a transverse coherence length of about 0.5 μm of the synchrotron radiation was assumed. The lateral distance between walls, D, practically does not change with depth, and is about 1000 interatomic distances. The change of mosaic spread with depth is thus solely related to the decrease of the misorientation angle due to the increase

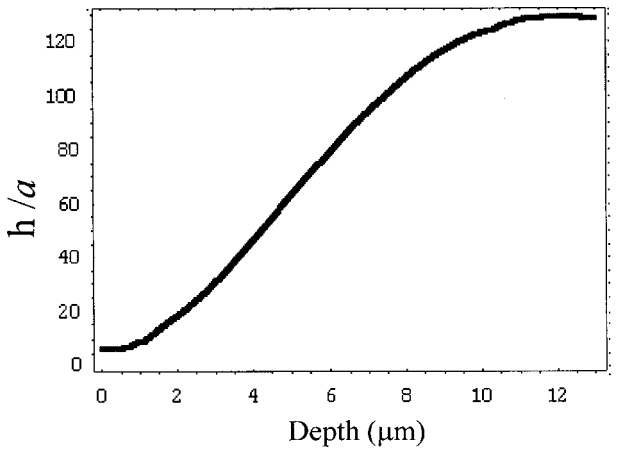

FIG. 5. Increase of the distance h/a (see the text) between dislocations inside the wall vs vertical depth corresponding to a depth-dependent change of the misorientation angle.

in the distance between dislocations within the wall. The functional dependence in Fig. 5 corresponds to the change of the misorientation angle with depth, as noted earlier, and creates a depth-dependent gradient of misorientations in the defective skin layer. One caveat should be noted: namely, our use of the term ''depth'' throughout this treatment refers, when compared with experimental data, to an absorption-weighted depth.

Finally, we should note, in discussing the two-length-scale pattern, that our analysis may also be useful where *both* length scales show a critical behavior. The above dislocation walls form regions with large-scale inhomogeneities with a characteristic size D. They create effective fields perturbing the crystal symmetry, and they destroy true long-range crystalline order in a three-dimensional crystal. With decreasing temperature, they result in a complicated state with different signs of the long-range order parameters in the regions adjacent to, or distant from, the walls. Following the approach given in Refs. 17 and 19, we can introduce a local transition temperature $T_0(r)$ and its fluctuations $\delta T_0 = T_0(r)\,\delta\tau_0$.

We can relate $\delta\tau_0$ to the distance between dislocation walls and to the distance between dislocations inside the walls. Fluctuations $\delta\tau_0$ in the presence of dislocation walls can be written as

$$\delta\tau_0 = \chi_0 b\phi\sqrt{\frac{1}{Dh}\ln\frac{D}{h}}, \quad \chi_0 = -K\frac{\partial T_c^0}{T_c^0 \partial P}. \qquad (12)$$

Here P is a pressure, K is the dilatation modulus, T_c^0 is a phase transition temperature for ideal crystal, ϕ is the orientation function for a dislocation and is of order unity. From Eq. (12), it follows that the temperature fluctuation behavior mainly depends on $\sqrt{1/Dh}$. As we demonstrated, the value h decreases on approaching the surface (Fig. 5), and fluctuations of the phase transition temperature become higher. Due to high fluctuations $\delta\tau_0$ in small regions of the crystal adjacent to a dislocation wall, locally ordered regions near the wall can appear at higher temperatures than the nominal critical temperature. *The influence of dislocation walls on a phase transition is much stronger than the influence of random dislocations*. As a result there exists a certain temperature interval $\tau_f > \tau \gg \delta\tau_0$, corresponding to the case where there are ordered regions near the dislocation walls occupying a relatively small volume of the crystal. The decrease of the distance between dislocations inside the walls near the surface (Fig. 5) results in a change of the conditions for the phase transition in the skin layer. Scattering off defects may thereby result in a narrow (more ordered) component, while scattering from critical fluctuations results in a broader component of the intensity distribution in a continuous phase transition. As a result, two-length-scale disk-shaped intensity distributions may appear near the appropriate reciprocal lattice points. Two length scales in the x-ray scattering from critical fluctuations were recently observed in $CuGeO_3$,[20] where the authors suggested that the effect is indeed due to dislocations in the skin layer.

In summary, we have clearly shown a network of dislocation walls corresponding to our experimental data. We were able to determine quantitatively the misorientation angle created by each dislocation wall as well as the distance h between neighboring dislocations inside the wall for different depths. We also have discussed a mechanism increase whereby fluctuations of the phase-transition temperature in the skin layer can be associated with dislocations. Nonetheless our principal purpose has been to provide a mechanism that can initiate the conversion of the order of the phase transition in our V_2H crystal from a first-order transition in the bulk to a continuous (tricritical) transition in the defective skin layer. By this we mean, as noted in Sec. I, that it is the applied strain field of the dislocation walls and its gradient that may drive the change of the order of the phase transition. The origin of the two length scales must therefore differ from prior work, in particular Ref. 20, as in V_2H it represents a change in the order of the transition.

This work was performed jointly at the University of Houston under the sponsorship of the National Science Foundation on DMR97-29297 and at the Max Planck Institute für Metallforschung, Stuttgart, where both R. B. and S. C. M. were visiting scientists; we thank both organizations for their support. We also wish to thank W. Donner for assistance with the paper.

[1] S. C. Moss, in *Electronic Structure and Properties of Hydrogen in Metals*, edited by P. Jena and C. B. Satterthwaite (Plenum, New York, 1983), p. 153.

[2] Y. Fukai, *The Metal-Hydrogen System* (Springer-Verlag, Berlin, 1993), Vol. 21.

[3] R. Hempelmann (unpublished).

[4] H. S. U. Jo, S. C. Moss, and D. G. Westlake, in *Modulated Structures–1979*, edited by J. M. Cowley, J. B. Cohen, M. B. Salamon, and B. J. Wuensch, AIP Conf. Proc. No. 53 (AIP, New York, 1979).

[5] J. Trenkler, S. C. Moss, H. Reichert, R. Paniago, U. Gebhardt, H. D. Carstanjen, T. H. Metzger, and J. Peisl, in *Proceedings of the International Advanced Studies Institute Conference on Exploration of Subsurface Phenomena by Particle Scattering (ASI-002), Monterey, CA, October 19–23* (1998), p. 155.

[6] B. Schönfeld, S. C. Moss, and K. Kjaer, Phys. Rev. B **36**, 5466 (1987).

[7] J. Trenkler, P. C. Chow, P. Wochner, H. Abe, K. E. Bassler, R. Paniago, H. Reichert, D. Scarfe, T. H. Metzger, J. Peisl, J. Bai, and S. C. Moss, Phys. Rev. Lett. **81**, 2276 (1998).

[8] J. Trenkler, H. Abe, P. Wochner, D. Haeffner, J. Bai, H. D. Carstanjen, and S. C. Moss, Modell. Simul. Mater. Sci. Eng. **8**, 269 (2000).

[9] A. L. M. Bongaarts and W. J. M. de Jonge, Phys. Rev. B **15**, 3424 (1977).

[10] W. B. Yelon, D. E. Cox, P. J. Kortman, and W. B. Daniels, Phys. Rev. B **9**, 4843 (1974).

[11] O. H. Seeck, D. Hupfeld, H. Krull, M. Tolan, and W. Press, Phys. Rev. B **58**, 623 (1998).

[12] J. Trenkler, Ph.D. thesis, University of Houston, Houston, 1999.

[13] J. Cardy and J. L. Jacobsen, Phys. Rev. Lett. **79**, 4063 (1997); A. N. Berker and G. Migliorini, Phys. Rev. B **57**, 426 (1998); J. Cardy, Physica A **263**, 215 (1999); N. S. Branco, Phys. Rev. B **60**, 1033 (1999); A. Kabakcioglu and A. N. Berker, Phys. Rev. Lett. **82**, 2572 (1999).

[14] M. Fähnle (private communication).

[15] L. Landau and I. Lifshitz, *Theory of Elasticity* (Pergamon, London, 1965).

[16] F. R. N. Nabarro, *Theory of Crystal Dislocations* (Dover, New York, 1987).

[17] M. Krivoglaz, *Theory of Scattering of X-Rays and Thermal Neutrons by Real Crystals* (Nauka, Moscow, 1987) (in Russian); p, 336; and in *Diffuse Scattering of X-rays and Neutrons by Fluctuations*, edited by S. C. Moss, J. Peisl, V. Baryakhtar, and M. Ivanov (Springer, Berlin, 1996).

[18] R. Barabash, Mater. Sci. Eng., A **309–310**, 49 (2001).

[19] I. M. Dubrovskii and M. A. Krivoglaz, Sov. Phys. Solid State **23**, 433 (1981).

[20] Y. J. Wang, Y.-J. Kim, R. J. Christianson, S. C. LaMarra, F. C. Chou, and R. J. Birgeneau, Phys. Rev. B **63**, 052502 (2001).